The Astronomical Journal, 157:45 (12pp), 2019 February https://doi.org/10.3847/1538-3881/aaf3b6

Circumstellar Dust Distribution in Systems with Two Planets in Resonance

Francesco Marzari[1], Gennaro D'Angelo[2], and Giovanni Picogna[3]
[1] Department of Physics and Astronomy, University of Padova, via Marzolo 8, I-35131, Padova, Italy; francesco.marzari@pd.infn.it
[2] Theoretical Division, Los Alamos National Laboratory, Los Alamos, NM 87545, USA; gennaro@lanl.gov
[3] Universitäts-Sternwarte München, Scheinerstraße 1, D-81679, Munich, Germany; picogna@usm.lmu.de
Received 2018 September 4; revised 2018 November 17; accepted 2018 November 21; published 2019 January 11

Abstract

We investigate via numerical modeling the effects of two planets locked in resonance, and migrating outward, on the dust distribution of the natal circumstellar disk. We aim to test whether the dust distribution exhibits peculiar features arising from the interplay among the gravitational perturbations of the planets in resonance, the evolution of the gas, and its influence on the dust grain dynamics. We focus on the 3:2 and 2:1 resonance, where the trapping may be caused by the convergent migration of a Jupiter- and Saturn-mass planet, preceding the common gap formation and ensuing outward (or inward) migration. Models show that a common gap also forms in the dust component similarly to what a single, more massive planet would generate and that outward migration leads to a progressive widening of the dust gap and to a decoupling from the gas gap. As the system evolves, a significantly wider gap is observed in the dust distribution, which ceases to overlap with the gas gap in the inner disk regions. At the outer edge of the gas gap, outward migration of the planets produces an overdensity of dust particles, which evolve differently in the 3:2 and 2:1 resonances. For the 3:2 resonance, the dust trap at the gap's outer edge is partly efficient, and a significant fraction of the grains filters through the gap. For the 2:1 resonance, the trap is more efficient, and very few grains cross the gap, while the vast majority accumulate at the outer edge of the gap.

Key words: planetary systems – planet–disk interactions – protoplanetary disks

1. Introduction

In the early stages of evolution of a planetary system, dust, gas, and planets may coexist. By probing the dust content of protoplanetary disks, ALMA and SPHERE observations of dust continuum emission have revealed the presence of gaps, rings, and spiral structures (e.g., Andrews et al. 2016; Isella et al. 2016; Feldt et al. 2017), which may represent signatures of planet–dust interactions. Small planets, not massive enough to carve a gap in the gas, may still be able to open gaps in the dust distribution due to their tidal torque. Exterior to the planet's orbit, the gravitational torque can counterbalance the aerodynamic drag torque, halting the inward drift of the dust. Interior to the planet's orbit, these torques add up and push the dust away, toward the star. Numerical and analytical modeling (e.g., Paardekooper & Mellema 2004, 2006; Rice et al. 2006; Zhu et al. 2014; Rosotti et al. 2016; Dipierro & Laibe 2017; Picogna et al. 2018; Ricci et al. 2018) explored this type of interaction and showed that planets with masses as low as $\approx 5\,M_\oplus$ (depending on the gas temperature and level of turbulence viscosity) can produce detectable signatures in a disk. The solid component of the disk has been modeled either as a dust fluid or using a large number of Lagrangian particles representative of the dust dynamics.

Characteristic features are more easily produced by the planet's tidal torque in the dust, rather than in the gas, distribution because the disk's gas is also subjected to a viscous torque, which tends to smooth out large density gradients (Pringle 1981). Planets massive enough to perturb the gas and open a gap in the gas distribution can create a pressure maximum at the outer gap edge, where dust particles can be trapped and pile up, enhancing the local density of the solids and producing a gap in the dust distribution around the planet's orbit. If dust is completely unable to filter through the gap, a cavity in the dust distribution develops. Depending on the disk's physical properties, already for masses larger than about $20\,M_\oplus$ (e.g., Lambrechts et al. 2014; Bitsch et al. 2018), a planet may be able to halt the inward flux of small solids and produce a cavity, observationally defined as a transition disk. According to Rice et al. (2006), for Jupiter-like planets, the filtration process is size-dependent, and dust grains typically smaller than 10 μm may cross the planet gap and reach the inner region of the disk, increasing the small particle population in the inner region of the disk. Because of their observational signatures, dust features can provide invaluable insights into the physics of planet–dust interactions and into the architecture of planetary systems.

In this paper, we focus on two giant planets, orbiting in a gaseous disk and locked in mean motion resonance (MMR), and explore the type of signatures they can impose on the dust distribution. A significant number of exoplanets are close to low-order resonances, like the 2:1 or 3:2 (Wright et al. 2011; Fabrycky & Kepler Science Team 2012). HD 45364 (Rein et al. 2010), KOI 55 (Kepler 70) (Charpinet et al. 2011), and other *Kepler* systems (Steffen et al. 2013) are suspected to be in 3:2 resonance while Gliese 876, HD 82943, and HD 37124 (Wright et al. 2011) are probably in 2:1 resonance. The K2-32 system hosts three planets near 3:2:1 resonances (Petigura et al. 2017). Many other systems may have been in resonance during their migration epoch, escaping from it at later times due to gas dissipation (Marzari 2018) and/or to gravitational interactions with leftover planetesimals (Chatterjee & Ford 2015).

A resonant configuration may be either the outcome of the formation process or a consequence of the early dynamical evolution of a planetary system. The formation of the first planet may trigger the growth of additional massive bodies in resonance, creating a resonance chain, like in Kepler 223 (Chatterjee & Tan 2014; Mills et al. 2016). A dynamical mechanism that may lead to resonant trapping of planets is convergent migration. If the outer planet migrates inward faster than the outer planet (Masset & Snellgrove 2001; Lee & Peale 2002), they eventually become

trapped in an MMR. The faster migration of the outer planet may be due, e.g., to its mass being lower than that of the inner planet. In the case of a Jupiter/Saturn-type pair, the exterior planet is unable to fully empty its co-orbital region, and its migration speed is similar to type I migration driven by corotation and Lindblad resonances (e.g., Tanaka et al. 2002). The inner planet, with a Jupiter mass or higher, will instead open a gap and drift inward at the typically slower rate of type II migration (e.g., D'Angelo & Lubow 2008; Ragusa et al. 2018, and references therein). The outer planet will approach the inner one and can be captured in an MMR, typically either the 2:1, the first to be encountered, or the 3:2 (more compact resonances are possible, but they require larger migration velocities during the approach phase). Once trapped in resonance, both planets may contribute to opening a common gap, possibly resulting in a regime of coupled migration.

The shape and depth of the common gap and the torques exerted on the pair of planets strongly depend on the type of resonance (either the 3:2 or the 2:1 MMR) and on the disk parameters (Masset & Snellgrove 2001; Lee & Peale 2002; Moorhead & Adams 2005; Thommes 2005; Beaugé et al. 2006; Crida et al. 2008; D'Angelo & Marzari 2012, hereafter DM12). Inward or outward migration may result, which is determined by the values of viscosity in the disk, the density and temperature profiles of the gas, and the masses of the two planets. Once captured in the MMR, the period of coupled inward/outward migration may continue until the disk eventually dissipates (assuming no interactions with other possible companions in the system). The "grand tack" scenario (Walsh et al. 2011) is a model based on this process. It was invoked to explain some features of the solar system, like the small mass of Mars and the compositional differences in the asteroid belt. It proposes that Saturn during its inward migration was trapped in either a 3:2 or 2:1 MMR with Jupiter (Morbidelli & Crida 2007; Pierens & Nelson 2008; DM12; Pierens et al. 2014). The formation of a common gap in the gas leads to a reversal of the torque sign, causing the interior planet to migrate outward, carrying the outer planet with it (via resonant forcing). The locked outward migration of the two planets continues as long as an appropriate torque imbalance can be sustained.

In this paper, we explore the evolution of dust particles in a circumstellar disk where two planets are trapped in resonance and migrate outward. We look for peculiar features in the dust distribution, related to this dynamical configuration, which might give rise to observable signatures in high-resolution images of disks acquired, e.g., with ALMA and SPHERE. The shape of the gap of two planets in resonance differs from that carved by a single one and the dust trapping at the outer border may change depending on the type of resonance. In addition, the outward migration of the planet pair may lead to the formation of morphological traits in the disk that can be detected in images and interpreted as due to two resonant planets. Two-dimensional (2D) hydrodynamical simulations of the outward migration of two planets in resonance, either in the 3:2 or 2:1 MMR, are performed, and the trajectories of solid particles of various sizes are integrated under the effect of drag forces induced by their interaction with the gas. In Section 2, we briefly summarize the dynamics of two planets embedded in a disk with their orbits locked in an MMR. In Section 3, we outline the numerical model and the initial setup of the simulations. In Section 4, we describe the evolution of the dust in the proximity of the common gap developed by a 3:2 MMR while, in Section 5, we focus on the 2:1 MMR. Section 6 is dedicated to the discussion of our results and conclusions.

2. Dynamical Evolution in the 2:1 and 3:2 Resonances

The most common scenario for the assembly of a 2:1 or 3:2 MMR is that the differential (convergent) orbital migration of two planets drives them into resonance. If the resonant forcing outweighs the tidal forcing, the orbits can become locked. Otherwise, convergent migration continues until either another resonance is encountered or dynamical instability ensues (Marzari et al. 2010). Since the planets orbit in a relatively compact configuration, the local thermodynamics conditions are similar in a smooth disk and, therefore, differential orbital migration typically requires that planets have different masses. Convergent migration also places some constraints on the disk's properties.

Analytical arguments (Quillen 2006; Mustill & Wyatt 2011) suggest that a less massive planet, of mass M_2, can be locked into the 2:1 orbital resonance with an interior and more massive planet, of mass M_1, if $|\dot{a}_2 - \dot{a}_1| \lesssim 1.2(M_1/M_s)^{4/3} a_2 \Omega_2$, where a_1 and a_2 are the planets' semimajor axes, and Ω_2 is the orbital frequency of the outer planet. Assuming that orbital migration is dominated by the type I (or a modified type I; D'Angelo & Lubow 2008, 2010) migration mode, DM12 found that the 1:2 resonance capture occurs when

$$\left(\frac{a^2\Sigma}{M_s}\right) \lesssim \left(\frac{H}{a}\right)^2 \left(\frac{M_s}{M_2}\right)\left(\frac{M_1}{M_s}\right)^{4/3}, \quad (1)$$

where Σ and H are the surface density and pressure scale height of the disk at around the outer planet's location. The predictions of the inequality above agree with results from direct hydrodynamical calculations of 2:1 resonance capture. For a given gas surface density, locking in the 2:1 MMR is more likely in warm disks, because of the slower (relative) migration velocity. If the inequality (1) is not satisfied, the tidal forcing can break the resonance, and another, more compact, resonant configuration may be established.

According to condition (1), the gas surface density required for capture in the 2:1 resonance is $\Sigma \lesssim 100$ g cm^{-2} in the 5 au region, when $H/a \approx 0.03$. For typical circumstellar disks, these densities are obtained after $\sim$0.5 Myr of evolution (DM12; see also D'Alessio et al. 2001), long before a Jupiter-mass planet can form (e.g., Lissauer et al. 2009; Movshovitz et al. 2010; D'Angelo et al. 2014).

One critical aspect of the 2:1 resonance is that the continued locked migration of the planets can lead to rapid growth of their orbital eccentricities (Lee & Peale 2002, 2003; Ferraz-Mello et al. 2003; Lee 2004; Teyssandier & Terquem 2014). If the mass ratio M_1/M_2 is similar to that of Jupiter and Saturn, i.e., $\approx$3.4, then the outer planet achieves a higher eccentricity. This was shown by Lee (2004) for various mass ratios of the planets. The peak values of eccentricity reached by the two planets depend on the damping effect caused by the gravitational interaction with the disk (Teyssandier & Terquem 2014). This outcome provides conditions on the disk density around the orbits of the two planets. Different eccentricities of the planets can lead to different gap shapes, which may significantly affect the dust density distribution in the disk where the gas eccentric perturbations are significant.

3. The Numerical Models

The evolution of a pair of planets interacting with a gaseous disk is simulated by means of the 2D FARGO code (Masset 2000), as modified by Müller & Kley (2012), which solves the Navier–Stokes equations for the disk on a polar grid (r, ϕ). We perform simulations where the energy equation includes viscous heating and radiative cooling through the disk surface

$$\frac{\partial E}{\partial t} + \nabla \cdot (E\,\boldsymbol{u}) = -P\,\nabla \cdot \boldsymbol{u} + Q^{+} - Q^{-}, \tag{2}$$

in which E and P are the total energy (surface) density and pressure, respectively, and $\boldsymbol{u}$ is the gas velocity field. In Equation (2), Q^{+} is the viscous dissipation term, computed from the components of the viscosity stress tensor (Mihalas & Weibel Mihalas 1999), which includes a physical kinematic viscosity and a von Neumann–Richtmyer artificial (bulk) viscosity, implemented as in Stone & Norman (1992) and where the coefficient defining the number of zones over which shock fronts are smeared out is set to 1.41. The term $Q^{-} = 2\sigma_{\rm SB}T_{\rm eff}^{4}$ is the local radiative cooling. The effective temperature $T_{\rm eff}$ is computed by using the Bell & Lin (1994) formulae for the Rosseland mean opacity, κ ($\sigma_{\rm SB}$ is the Stefan–Boltzmann constant).

The trajectories of small dust grains with sizes 10 μm, 100 μm, 1 mm, and 1 cm, for a total of 4×10^{5} particles, are integrated along with the hydrodynamical evolution of the gas. Although the largest-size particles do not strictly qualify as dust grains in the typical context of the interstellar medium (Draine 2011), we model them because of their importance in the context of protoplanetary disks and refer to them as grains for simplicity. These grain sizes represent typical values that can be detected by ALMA in the infrared. The aerodynamic forces acting on the dust particles are computed as in Picogna & Kley (2015). The drag force acting on a spherical dust particle of radius s, moving with a velocity $\boldsymbol{v}$ relative to the gas, is given by

$$\boldsymbol{F}_{D} = (1-f)\boldsymbol{F}_{D,\rm E} + f\boldsymbol{F}_{D,\rm S}, \tag{3}$$

where

$$\boldsymbol{F}_{D,\rm E} = -\frac{4}{3}\pi s^{2}\rho_{g} v_{\rm th}\boldsymbol{v} \tag{4}$$

$$\boldsymbol{F}_{D,\rm S} = -\frac{1}{2}\pi s^{2} C_{D}\rho_{g} v\boldsymbol{v} \tag{5}$$

are drag forces in the Epstein and Stokes regimes, respectively. In Equation (4), $v_{\rm th} = \sqrt{8k_{\rm B}T/(\pi\mu m_{\rm H})}$ is the mean thermal velocity of the gas molecules, T the local temperature of the gas, ρ_{g} the gas volume density, $m_{\rm H}$ the hydrogen atom mass, and μ the mean molecular weight of the gas. The drag force in the Stokes regime is proportional to the drag coefficient, C_{D}, whose value is taken from Weidenschilling (1977) and depends on the Reynolds number. The transition between the two drag forces is determined by the coefficient f, given by

$$f = \frac{s}{s+\lambda} = \frac{1}{1+{\rm Kn}}, \tag{6}$$

where λ is the mean free path of the gas molecules and ${\rm Kn} = \lambda/s$ is the Knudsen number. Comparing the expressions for $\boldsymbol{F}_{D,\rm E}$ and $\boldsymbol{F}_{D,\rm S}$, it can be shown that they are equal when ${\rm Kn} = 4/9$ for Reynolds numbers <1 (see Weidenschilling 1977). Due to drag forces, particles experience a radial drift relative to the gas, and they also respond to density and velocity gradients in the gas. The drift velocity (relative to the gas), in conditions of stationary gas surface density, can be approximated as (Birnstiel et al. 2010; Pinilla et al. 2012)

$$v_{\rm drift} = \frac{1}{{\rm St}^{-1} + {\rm St}}\left(\frac{\partial P}{\partial r}\right)\frac{1}{\rho_{g}\Omega}. \tag{7}$$

Indicating with m_{s} the mass of a particle, ${\rm St} = m_{s}v\Omega/\boldsymbol{F}_{D}$ represents the Stokes number (sometimes referred to as non-dimensional stopping time) and Ω the Keplerian frequency of the disk. Since $v_{\rm drift}$ depends on the radial derivative of the gas pressure P, any local pressure maximum in the disk (with a significant azimuthal extent) will collect and trap grains, both orbiting in the vicinity of the maximum and those drifting inward from the outer disk regions. Under barotropic conditions, a local pressure maximum translates into a density maximum that generates locations where dust grains can be confined and, as a result, where their density may increase. The common gap formed by two resonant planets can produce such confinement locations, in particular at its outer border.

Additional calculations are performed with the code employed by DM12, which applies an orbital advection scheme implemented along the lines of the algorithm described by Masset (2000). Further details are given in DM12. The thermodynamical evolution of the solids interacting with the gas, the planets, and the star is calculated using the methods and algorithms described in D'Angelo & Podolak (2015). The code computes the motion of solids through the gas and their thermal state in a self-consistent fashion, including ablation and break up. The small solids considered here are basically isothermal and in thermal equilibrium with the gas. Since they are typically very well coupled to the gas, frictional heating is small, and their thermal budget is mainly dictated by heating in the gas thermal field and by radiative cooling. Due to the low velocities relative to the gas, the dynamical pressure exerted by the gas is typically not sufficient to break up the solids. Since the particles modeled here are made of silicates and their temperature does not exceed a few hundred Kelvin degrees, ablation is negligible. In some test cases under the same initial conditions, the two codes provided very similar results. Therefore, we decided to use the FARGO code for most of the computations discussed herein.

3.1. The Disk Setup

The shape and depth of the common gap developed by a pair of planets and the outward (inward) migration rate are strongly dependent on the values of the disk viscosity, density and temperature profiles of the gas, and masses of the two planets (Masset & Snellgrove 2001; DM12). Performing a full exploration of all these parameters, along with the study of the dust evolution, is outside the scope of this work. We instead focus on models in which the planets become locked in either the 3:2 or 2:1 MMR and migrate outward. The investigation of the dust evolution in these models is performed with the goal of highlighting some effects that may represent a common outcome of resonant pairs undergoing outward migration. Although some calculations resulted in inward migration after

resonance locking of the planet pair, here we only report on the effects of outward migration on the dust particle distribution.

To model the circumstellar disk with FARGO, we adopt a polar, (r, ϕ), grid with 720×360 elements uniformly covering the disk, which extends from $r = 0.5$ au to 15 au from the star. The initial gas density profile is given as

$$\Sigma(r) = \Sigma_0 \left(\frac{r}{\mathrm{au}}\right)^{-p} \mathrm{g\ cm^{-2}}. \quad (8)$$

When modeling the 3:2 MMR, we consider two density values, $\Sigma_0 = 750\ \mathrm{g\ cm^{-2}}$ and $\Sigma_0 = 1000\ \mathrm{g\ cm^{-2}}$, and the slope of the density distribution (i.e., the power index) is set to $p = 1$. For the 2:1 MMR, we consider instead only $\Sigma_0 = 750\ \mathrm{g\ cm^{-2}}$ and $p = 3/2$. These parameters are chosen (based on several experiments) to ensure a sustained outward migration of the two planets once they are locked in resonance. It is noteworthy that for smaller values of Σ_0, i.e., $\Sigma_0 < 500\ \mathrm{g\ cm^{-2}}$, capture is always in the 2:1 MMR, and the migration is directed inward regardless of the power index p (that was applied).

The values adopted for Σ_0 are smaller than those predicted for the Minimum Mass Solar Nebula (Weidenschilling 1977; Hayashi 1981) because they are presumed to take into account the time required by the planets to grow. During this time, the disk is partially dissipated by the viscous evolution and, possibly, by photoevaporation. Nonetheless, these values correspond to an initially relatively massive protoplanetary disk. In fact, allowing 0.5–1 Myr for the two planets to form and 3–4 Myr for the disk's gas to disperse, the initial disk mass can be as large as $\sim 0.1\, M_\odot$ (DM12).

The disk aspect ratio is initialized to $h = H/r = 0.02$. The shear kinematic viscosity is $\nu = \alpha H^2 \Omega$, where the turbulence parameter is a constant, $\alpha = 10^{-4}$ or 10^{-3} for the 3:2 MMR and $\alpha = 10^{-4}$ for the 2:1 MMR. This initial setup is similar to that adopted by Pierens et al. (2014), in which the authors study the outward migration of Jupiter and Saturn in cold disks. When the planets are fully formed, the host disk is possibly evolved and may be characterized by a low viscosity. Both these factors may lead to a disk with a small aspect ratio ($h \approx 0.02$). Regardless, in the present case, this small value is required to drive outward migration when the planets are trapped in a 2:1 resonance. Warmer, more viscous disks do not typically induce outward migration of the pair of planets, but rather inward migration (DM12). This condition on the aspect ratio can be relaxed for the 3:2 resonance, which may drive outward migration even for large aspect ratios ($h = 0.05$; Masset & Snellgrove 2001; DM12).

Note that since the gas temperature evolves according to Equation (2) and $H\Omega = \sqrt{k_\mathrm{B} T/(\mu m_\mathrm{H})}$, the kinematic viscosity, ν, is proportional to T, and therefore varies with time, both globally and locally around the planets.

Convergent migration determines which resonance is established. According to condition 1, in cold disks, it is more likely to overcome the 2:1 resonance locking. In an unperturbed and stationary disk, the energy balance in Equation (2) reduces to

$$Q^+ \approx Q^-, \quad (9)$$

where viscous heating can be approximated to $Q^+ \approx 9/4 \Sigma \nu \Omega^2$, and radiative cooling is $Q^- \approx 32 \sigma_\mathrm{SB} T^4/(3\kappa\Sigma)$ (assuming that the optical thickness to the disk midplane is $\kappa\Sigma/2$). At low temperatures ($T \lesssim 200$ K), dust opacity is dominated by ice grains and $\kappa \approx \kappa_0 T^2$ (e.g., Bell & Lin 1994). Therefore, $T \propto \alpha\Sigma^2\Omega$ and $H^2 \propto \alpha\Sigma^2/\Omega$, which entail the possibility of local variations of the pressure scale height in the proximity of the planets, possibly affecting the dynamics of both the planets and the dust. Note that the situation is quite different in a locally isothermal disk, in which H depends on r but remains constant in time and does not respond to local perturbations of the gas exerted by the planets.

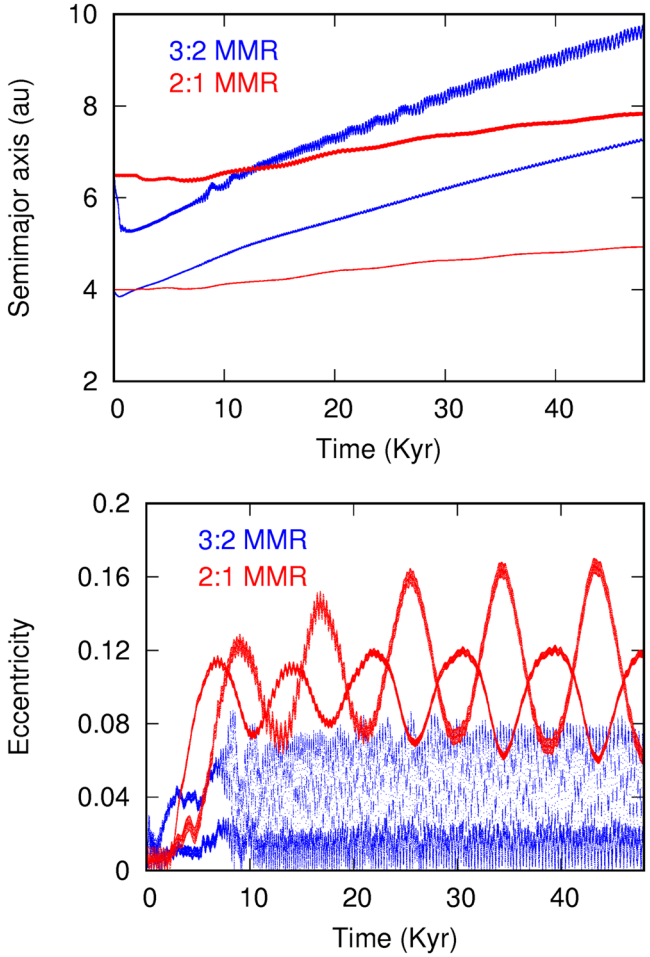

Figure 1. Time evolution of the semimajor axis (top) and eccentricity of the two planets locked in a 3:2 (blue lines) and 2:1 MMR (red line). The gas density profile declines as r^{-1} in the first case and as $r^{-3/2}$ in the second case. The migration in the 3:2 MMR case is faster also due to the larger density around the planets' locations.

Figure 1 shows the semimajor axis and eccentricity of the inner and outer planets in the two different cases. The outcome of the resonance locking (top panel) is in general agreement with the inequality (1), which predicts densities somewhat lower than $40\ \mathrm{g\ cm^{-2}}$ at $r \approx 6$ au for capture in the 2:1 resonance. To within factors of order unity, the agreement is reasonable also for the case with density slope $p = 3/2$ (red lines).

When the planets are locked in 3:2 resonance (blue lines), their eccentricities remain low during the outward migration, and the eccentricity of the inner planet stabilizes around 0.01 while that of the outer planet is on average $\approx$0.05. In the case of the 2:1 MMR, where the slope of Σ is $p = 3/2$, the eccentricities of the two planets grow on a short timescale to

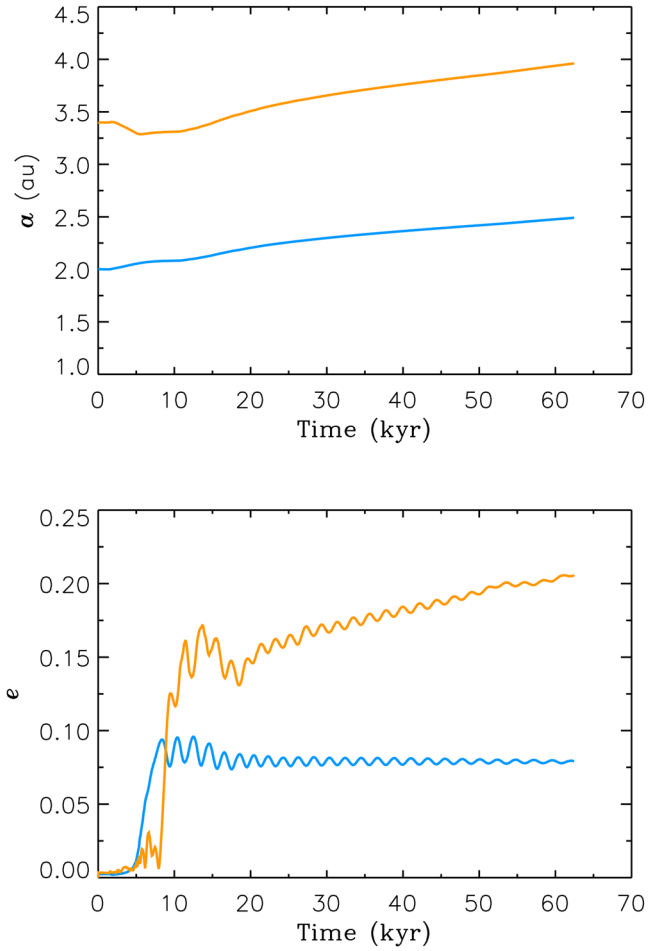

Figure 2. Semimajor axis (top) and orbital eccentricity (bottom) evolution of a Jupiter–Saturn-mass pair converging into 2:1 MMR and migrating outward thereafter. The more massive planet is on the interior orbit. This isothermal simulation is perform with the second code discussed in Section 3.

0.09 and ≈0.12 for the inner and outer planets, respectively, and evolve through cycles of large anticorrelated oscillations.

To test the robustness of the migration scenario, we performed an additional calculation carried out with the other code discussed in Section 3, and the results are illustrated in Figure 2. In this model, the disk is flared and locally isothermal with $H/r = 0.024(r/\mathrm{au})^{2/7}$; the kinematic viscosity is $\nu = 4 \times 10^{-8}$ in units of Ωr^2 at $r = 1$ au, corresponding to $\alpha = 10^{-4}$ at 1 au. Referring to Equation (8), the gas surface density is such that $\Sigma_0 = 530\ \mathrm{g\ cm^{-2}}$ and $p = 3/2$. The disk extends radially from 0.25 to 54 au, with a resolution $\Delta r = \Delta\phi/r = 0.01$. As expected from condition (1), convergent migration drives the pair of planets in the 2:1 MMR (top panel). After the resonance is established, gap overlap drives the pair outward. Similarly to the cases shown in Figure 1, the inner planet acquires an orbital eccentricity ≈0.08, whereas the eccentricity of the outer planet increases beyond 0.2 (bottom panel). These results are overall consistent with those discussed above, implying that the details of the disk structure may not be critical to the outcome, as long as the gas is cold and has low viscosity.

Note that the interior, Jupiter-mass planet in Figure 2 starts to migrate outward when "released" (tidal torques start acting on the planets only 1500 years after the beginning of the simulation, to allow for an initial relaxation period), prior to the onset of the resonance locking. The reason for this behavior is probably related to tidal interactions with a cold and low-viscosity gas, which induces eccentric perturbations in the disk that result in a positive torque exerted on the planet (D'Angelo et al. 2006). A similar behavior can also be seen in the top panel of Figure 1 (red lines).

The eccentricity evolution in the 2:1 resonance displayed in the bottom panel of Figure 1 also shows large-amplitude oscillations that are not seen in the evolution illustrated in the bottom panel of Figure 2. This is likely due to the local-isothermal approximation used in the latter model. The disk is warmer, and the kinematic viscosity is not affected by disk temperature. This is not the case in the models of Figure 1, which tend to have lower aspect ratios around the orbits of the planets, and the kinematic viscosity depends on the disk temperature. The smaller values of H/r and ν tend to enhance the eccentricity of the disk's gas (both in strength and spatial domain; D'Angelo et al. 2006). The exchange of eccentricity between the planet's orbit and the disk, compounded with the resonant forcing between the planets, may be responsible for the resulting variations in the planet's eccentricity evolution.

4. The 3:2 Resonance

By applying an initial surface density with power index $p = 1$ and $\Sigma_0 = 750\ \mathrm{g\ cm^{-2}}$, the two planets become trapped in a 3:2 MMR and migrate outward thereafter. A common gap is formed in the gas distribution as a result of the tidal interaction between the planets and the disk. The common gap moves along with the planets while their orbital eccentricities remain small (see Figure 1).

To test the formation of a common gap also in the dust distribution, we first run a simulation in which the planet masses grow on a timescale of 10^3 years, until they attain their final values. The dust particles are introduced in the simulation from the beginning and they evolve under the influence of gravitational and drag forces, and are affected by the formation of the gas gap during and after capture in resonance. The initial dust distribution extends from 2 to 15 au from the star, and all dust grains migrating inside of $r = 2$ au are discarded from the simulation to reduce the computing time. Figure 3 shows dust spatial distributions after 20 kyr. A gap in the dust distribution forms, for all particle sizes considered here (from 10 μm to 1 cm), overlapping the gas gap created by the pair of planets in MMR. The dust gap is not completely empty, since some grains are trapped in the co-orbital regions of both orbits, possibly because of the assumed fast growth of the planet masses (Marzari & Scholl 1998).

In Figure 3, we only plot the spatial distributions of 10 μm and 1 cm size particles. In fact, while grains in the size range between 10 μm and 1 mm show a similar evolutionary behavior in terms of spatial distributions, 1 cm grains drift inward at a significantly faster speed, producing a different spatial distribution. The different evolution can also be predicted on the basis of Figure 24 of Armitage (2017), showing the radial drift timescale, t_{drift}, as a function of the Stokes number. Under physical conditions similar to ours ($\alpha \approx 0.001$), particles in the size range from 10 μm to 1 mm have Stokes numbers ranging from 10^{-5} to 10^{-3}, with a predicted t_{drift} from about 7 to 3 times 10^5 in units of the orbital period. The radial drift timescale quickly drops to about 2×10^4 for a Stokes number of 10^{-2}, corresponding to our 1 cm size particles. The difference in t_{drift} explains various features in Figure 3:

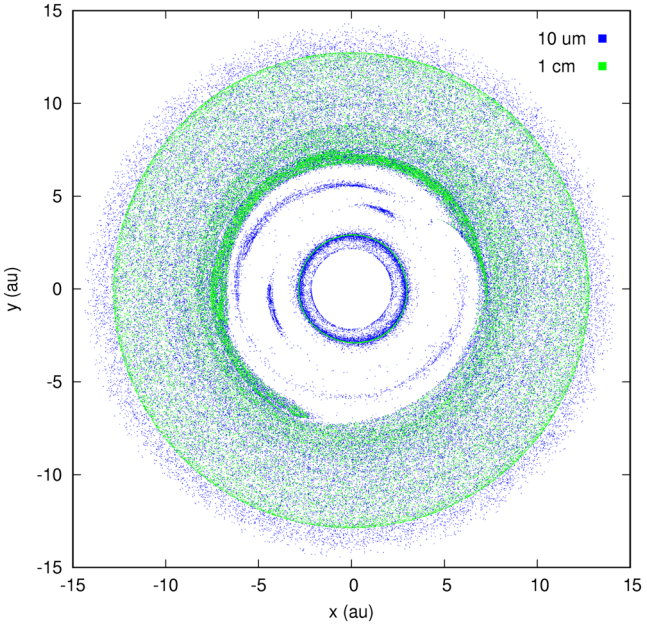

Figure 3. Dust distribution after 20 kyr of evolution. A gap forms in the dust distribution and some dust is trapped in the co-orbital regions of the planets. The particles shown in the plot have radii of 10 μm and 1 cm and Stokes numbers of 10^{-5} and 10^{-2}, respectively. While particles with size from 10 μm to 1 mm show a similar evolution, 1 cm size grains exhibit some morphological differences in the spatial distribution compared to the smaller ones.

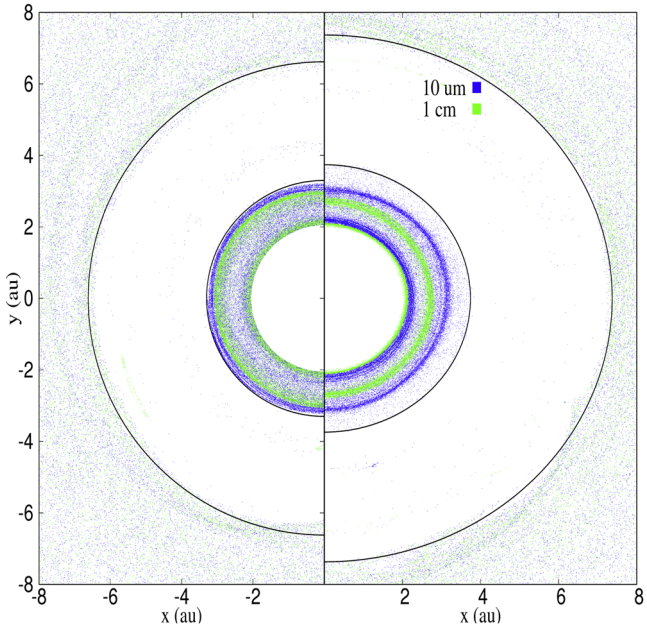

Figure 4. Initial dust distribution (left side) and after 20 kyr (right side). The black dashed lines show the edges of the common gas gap produced by the planets on resonant orbits. Notice how the dust gap broadens as the planets migrate outward. Particles of 10 μm and 1 cm radius are plotted. The larger, 1 cm size grains also drift inward at a rate comparable to the outward migration rate of the planets, visibly increasing the extent of the corresponding gap in the dust (green dots).

(1) the outer edge of the dust disk is mostly populated by smaller grains, (2) there is an overdensity of 1 cm grains at the outer border of the gap, and (3) the inner region of the gap is partly depleted in large grains that have already migrated inside 2 au (and therefore removed from the numerical model).

The outcome of this numerical simulation confirms that the common gap in gas leads to the formation of a similar gap in the dust distribution and that the two gaps approximately overlap at the beginning of the evolution. The dust trapped within the gap in horseshoe orbits is probably short-lived because the trajectories are unstable. However, if the collision rate is large enough, these particles may accumulate into larger bodies at Trojan locations before drifting toward the inner disk.

We acknowledge that this model must be considered only as indicative of the dust gap formation. It is difficult to simulate a more realistic evolution of the system. In particular, the mass growth of the planets, which is assumed in this model, occurs on a relatively short timescale. In fact, the growth timescale is set by disk-limited accretion (Lissauer et al. 2009), which depends on the thermodynamic state of the disk and disk–planet tidal interactions. In a cold and low-viscosity disk, the growth rate may be significantly longer.

In addition, giant planet cores may be massive enough to already form dust gaps prior to resonant trapping (Picogna & Kley 2015; Dipierro & Laibe 2017). However, we would not expect these effects to significantly change the dynamical evolution of the dust. Therefore, for the thermodynamical gas conditions used in the model, we would still expect the formation of a common gap in the dust as illustrated in Figure 3.

To explore the later stages of dust evolution during the outward migration of the planets, we run different simulations in which the planets and the gaseous disk evolve until the resonant state is established and outward migration ensues. Once the planets have migrated outward for some time, we introduce dust particles in the simulation, either interior or exterior to the common gas gap, and compute their evolution over a long time period. A different behavior is observed close to the inner and outer borders of the gas gap, due to the diverse coupling between the gravity and drag forces acting on the particles.

The gas gap, shifting as the planets migrate outward, leads to a progressive radial (outward) migration of the gap edges. At the inner border, gas streaming through the gap from the outer disk refills the region left empty by the outward movement of the edge. The dust, however, unable to efficiently filter through the planets' orbits, does not replenish the portion of the disk left devoid of dust by the outward shift of the inner gap edge. As a result, the inner border of the dust gap is left behind while the planets and the gas gap move outward.

This different behavior of the dust and gas can be observed in Figure 4. The initial dust distribution on the left side evolves in the spatial distribution shown on the right side, after about 20 kyr. Also in this case, we use the 10 μm grains as representative of the distribution of particles in the range 10 μm–1 mm, and 1 cm particles whose drift rate is significantly higher. The gap in the dust distribution becomes wider over time and decouples from the gas distribution around the gap region. The effect is more marked for 1 cm size particles since, during the outward migration of the gas gap, they also drift inward at a comparable rate, increasing the width of the dust gap. The dust evolution leading to a broader gap may complicate the interpretation of high-resolution observations of dust distributions in disks, like those obtained with ALMA. The width of the gap is used to estimate the masses of the planets. But in an outward migration scenario as that represented here, the dust gap is broader than it would be in the static, i.e., non-migrating, case. Therefore, to match the observed gap width, planets more massive than necessary

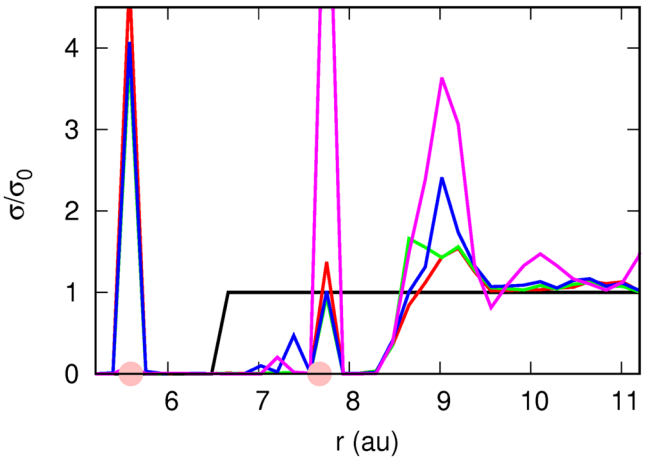

Figure 5. Histogram of the dust radial distribution after 20 kyr from its inclusion in the simulation. The particles are initially located in the outer region of the disk, bordering the gap's exterior edge. Along the y-axis, we plot the ratio between the initial dust density, σ_0, and the final dust density, σ, as a function of the radial distance. The black line marks the initial distribution of dust while the red, green, blue and magenta lines indicate the distribution after 20 kyr of 10 μm, 100 μm, 1 mm, and 1 cm size particles, respectively. As the gas gap moves outward, the dust develops an increasing density peak at the exterior border, which is more marked for largest grains due to their fast inward drift. The planet positions at the end of the simulation are marked by filled pink circles.

would be invoked. It is noteworthy that the orbital eccentricities of both planets remain below 0.1; therefore, the observed effect is not due to the increased radial excursion of the planets (which would result in eccentric gap edges; D'Angelo et al. 2006). We also expect a gap width that depends on the observed grain size, which may provide an important test to characterize the type of planetary system responsible for gaps in the dust distribution.

In the long-term evolution, the strongly reduced inward dust flux across the planets' orbit and the radial drift of the dust relative to the gas would lead to the formation of a cavity, even in the absence of outward migration. The formation timescale, however, would be relatively long compared to that due to the planet migration in this resonance. Also, it would depend on the Stokes number of the dust (see Figure 24 of Armitage 2017).

An additional effect of the outward migration of the common gas gap is the accumulation of dust particles at its outer border. As the planets move outward, the exterior edge pushes the dust outward, locally collecting solids and generating an overdense dust region around the exterior border of the gas gap. Over time, this region of enhanced density moves outward, carried by the expanding gas gap edge. As a result, dust concentrations may rise significantly and attain levels much higher than those expected from the mere accumulation of particles due to inward drift driven by gas drag, because it may occur on a much shorter timescale (i.e., the migration timescale of the planets). This is especially the case for small grains, which have very low (drag-induced) drift velocity relative to the gas, and observational evidence of such features may be indicative of a planet migrating outward.

The process of dust accumulation along the exterior edge of the gap is shown in Figure 5, where the dust density is derived by grouping the test particles in radial bins. In the figure, the dust density σ is normalized to the initial dust distribution, σ_0, derived from the positions of the particles at the beginning of the simulation. The ratio σ/σ_0 is computed as a function of the radial distance, and it is assumed that the initial dust-to-gas mass ratio is constant. In this way, we ignore the effects of the frost line, which, however, can be easily accounted for with a renormalization of the dust density. The distribution of different grain sizes is shown in different colors and, as expected, for 1 cm particles, the overdensity is markedly higher due to the contribution of their rapid inward drift.

The growing density peak at the exterior edge of the shifting gas gap, which also depends on the grain size, may provide useful observational evidence for a pair of planets migrating outward. If the column density of small dust displays an anomalously large peak at the outer edge of a gap observed in a disk (e.g., with ALMA or possibly with the Next Generation Very Large Array), this may indicate a "sweep-up" effect of two planets locked in 3:2 resonance and migrating outward.

Just inside the outer edge of the gap where the gas density acts as a dust trap, two additional large peaks in the dust density form in the proximity of each planet, where a significant amount of dust seems to be collected around them. For this particular resonance (we will see that this does not occur in the 2:1 resonance case), the dust barrier at the exterior edge is not fully efficient, and a non-negligible fraction of dust filters through the outer edge of the gap during the coupled migration of the planets.

This effect can be seen in Figure 6 by comparing the distribution of the gas and that of the dust particles. They filter through the gap edge, entrained in the gas streams, and reach the vicinity of both planets where they become trapped in bound orbits, and possibly accrete on the planets. The enhanced concentration of dust in the accreted gas may impact the growth rate of the planets if it significantly raises the opacity of the envelope gas. It is noteworthy that 1 cm size particles filtering through the outer edge of the gap are almost all captured by the exterior planet (see Figure 5), whereas most of the smaller grains are captured by the interior planet. This difference is due to the different amount of coupling between particle and gas dynamics.

We performed an additional simulation in which the initial density of the gas is increased by about 30%, $\Sigma = 1000(\mathrm{au}/r)\,\mathrm{g\,cm^{-2}}$, and the kinematic viscosity is characterized by $\alpha = 10^{-3}$, 10 times higher than in the simulation discussed above. In this scenario, the outward migration is enhanced (because of the larger density), and the overall disk temperature is higher as well. The tidal perturbations exerted by the planets on the gas are countered by more vigorous viscous torques, which reduce their strength and facilitate the transit of dust through the gap and toward the inner region of the disk. In Figure 7, the dust distribution is shown after about 15 kyr from the inclusion of the particles in the model. In the outer region of the disk, the usual density peak is observed due to dust accumulation. Smaller particles from 10 μm to 1 mm in size accumulate at the exterior border but, as in the previous case (see Figure 5), a significant fraction of them filter through the gap edge following the gas flow. Some are trapped by the interior planet while most of them cross both orbits and produce an additional peak around 5 au. The radial location of this inner peak is time-dependent and determined by the drift velocity of the particles. The interpretation of the complex features observed in Figure 7 for the smaller grains may be problematic because the disk would appear to be separated into three dust rings, which might be attributed—erroneously—to a

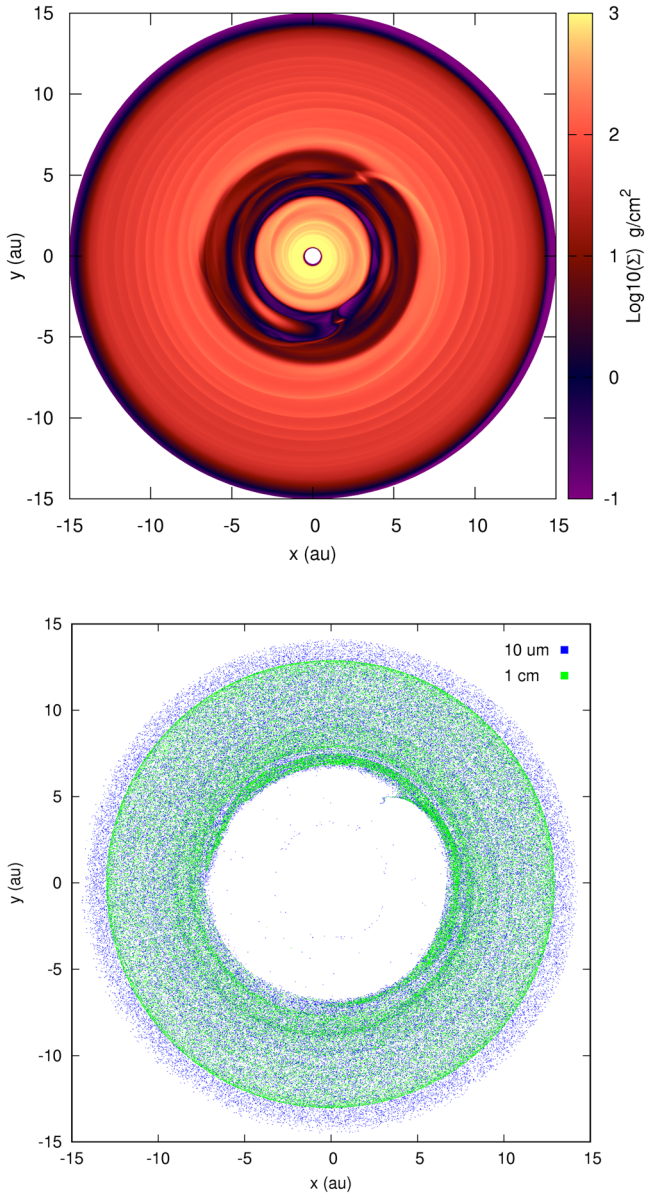

Figure 6. Gas density distribution (top) and dust spatial distribution (bottom) after 10 kyr from the beginning of the simulation. Dust particles are entrained within streams crossing the planets' orbits and then become trapped around them.

massive planet located around 7 au and by an additional less massive planet located around 4 au. In reality, the planets are located within the main dust gap and are migrating outward.

The larger, 1 cm grains show a different behavior compared to the smaller ones. A significant fraction of particles drift through the exterior edge of the gas gap and end up in the close proximity of the planet, as in the previous case. Therefore, they do not contribute to the secondary peak observed for the smaller grains around 5 au. At the outer edge, a large overdense region builds up because of the combination of the outward migration of the gap and of the inward radial drift of the grains. An additional outer peak is present in the radial distribution, and it is caused by a small increase of the Stokes number toward the outer regions of the disk, due to the thermo-dynamical structure of the disk. This small increase leads to a faster drift of the particles, which can overtake the inner ones, producing the smaller peak observed in the dust distribution

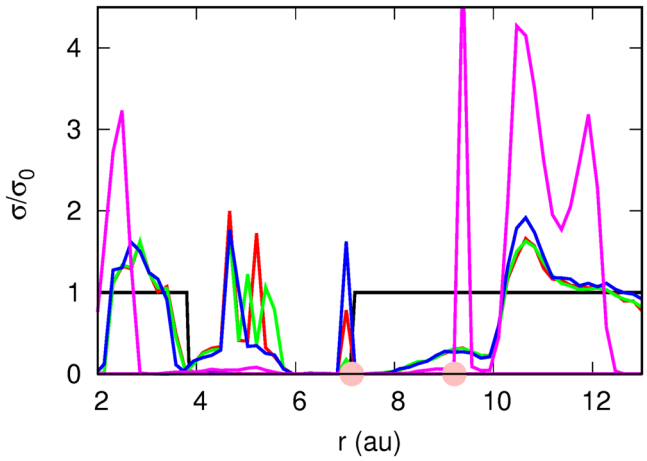

Figure 7. Histogram of the dust radial distribution 15 kyr after the inclusion in the simulation with $\Sigma = 1000(\mathrm{au}/r)$ g cm^{-2}. The particles are initially located in the inner and outer regions of the disk bordering the edges of the gas gap. As in Figure 5, the y-axis indicates the dust density normalized to its initial value, σ_0, as a function of the radial distance. The different lines are as in Figure 5.

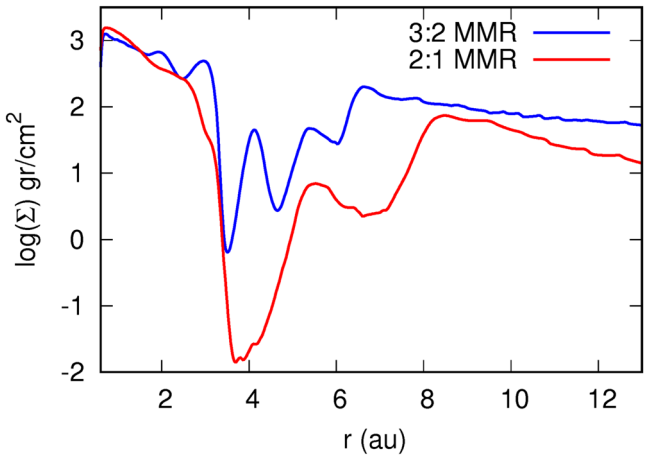

Figure 8. Common gap carved by the planet pair locked in the 3:2 (blue) and the 2:1 MMR (red). In the latter case the planet separation is larger and their eccentricities are higher, causing the gap to be wider.

around 12 au. This additional feature is not observed in the distribution of the smaller grains because they drift inward at a lower speed, and their evolution is mostly dominated by the outward drift of the gas gap. This different dynamical evolution related to the size of the particles may represent an additional test to identify the presence of planets in resonance.

5. The 2:1 Resonance

When the power index of the gas density in Equation (8) is equal to $p = 3/2$, the two planets become trapped in a 2:1 MMR because of the lower gas density at the planets' locations (see Equation (1)). For the chosen disk conditions, the pair migrates outward, but at a slower speed compared to the 3:2 MMR cases discussed in the previous section. The resonant forcing, however, has a stronger effect on the orbital eccentricities of the planets than in the previous cases (see Figure 1). The wider separation between the planets, combined with their higher orbital eccentricity, leads to a gas gap for the 2:1 MMR case that is broader than that of the 3:2 MMR, as illustrated in Figure 8.

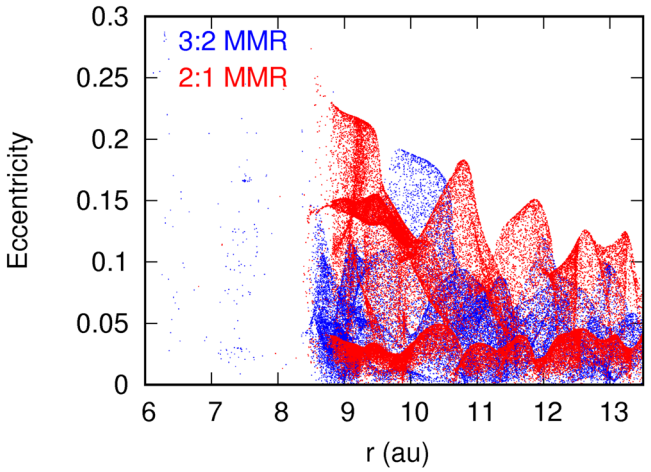

Figure 9. Distribution of the dust particle eccentricities close to the outer edge of the gap for the 3:2 (blue) and 2:1 MMR (red), respectively. The evolutionary times are different for the two resonances and are selected in order to have the gap outer edge at similar locations and to compare the grain eccentricity values at similar distances from the star.

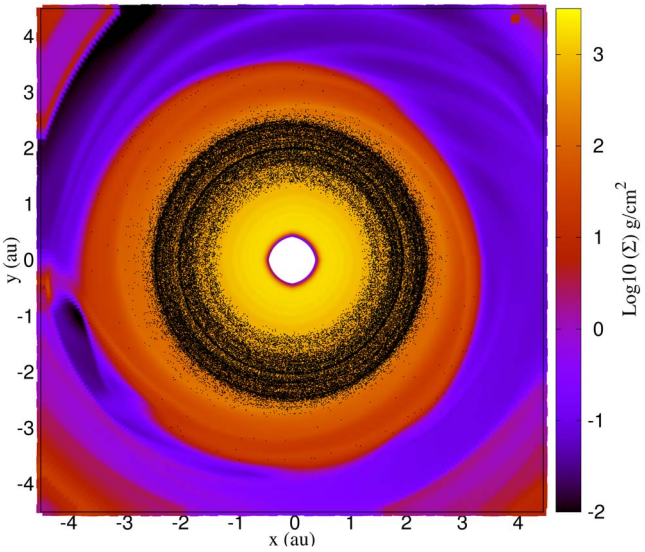

Figure 10. Gas density distribution and dust particles (only those of 10 μm in radius) in the inner region of the disk after 30 kyr of outward migration of the planets, locked in the 2:1 MMR. The dust particles are marked by black dots.

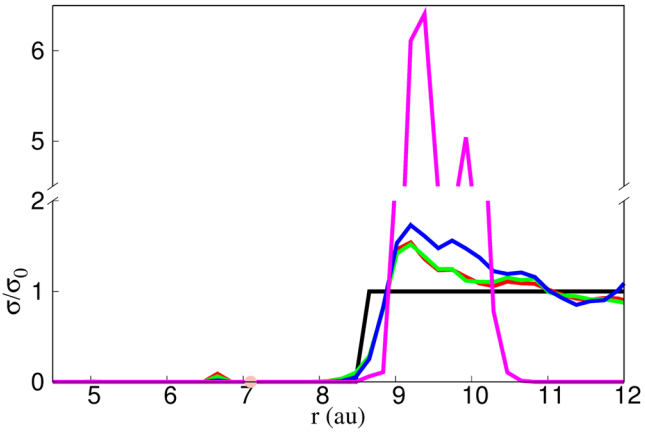

Figure 11. Histogram showing the normalized distribution of dust particles after 30 kyr of evolution within the disk. Dust accumulates at the exterior border of the gas gap, creating a dense dust ring, which can be detected by observations. Its density is significantly higher compared to the case of the 3:2 MMR (for similar evolution times), also taking into account the slower outward migration rate of the planets.

The gap also appears deeper than in the 3:2 MMR case, but this may be due to the different evolutionary times of the two configurations shown in the figure. Since the speed of the outward migration for the 3:2 MMR case is faster than in the 2:1 MMR case, to compare the gaps at similar locations in the disk, different evolutionary times were chosen for the two cases illustrated in Figure 8. The gap in 2:1 MMR is significantly more evolved, which is consistent with its greater depth. The lower migration speed of the 2:1 MMR case also contributes to make the gas gap deeper.

The higher eccentricity of the planets affects not only the morphology of the gaseous disk but also the orbital parameters of the dust grains. In Figure 9, the eccentricities of the dust particles in 3:2 and 2:1 resonance are compared at different evolutionary times during the planets' outward migration, when the exterior border of the gaps in the dust are approximately equal. In the configuration shown, the planets are at different radii (in the two simulations), but the radial locations where dust is collected are similar in the two cases because the gap generated by the 2:1 MMR locking is broader. Additionally, in the case of the 2:1 MMR, the dust grains move on more eccentric orbits compared to the 3:2 MMR case, in particular close to the gap edge.

Notwithstanding the different shapes of the gaps and eccentricities of the particles, the same phenomenon observed in the gap region of the planets in 3:2 MMR takes place in the 2:1 MMR case. The dust particles populating the inner disk are not replenished as the planets migrate outward, so that the inner edge of the dust gap appears to recede from that of the gas. However, this happens on a longer timescale compared to the 3:2 MMR case, because the outward migration of the planets is slower. Also, in the 2:1 MMR case, the gap in the dust progressively broadens as the planets migrate outward while that of the gas remains approximately constant (over the same timescale). This effect is clearly shown in Figure 10, where the dust particles are plotted against the gas density distribution. After 20 kyr from the inclusion of the dust grains in the calculations, the gap has significantly moved outward and the gas has refilled the volume left empty by the outward movement of the inner planet. The dust, however, behaves differently, and the initial ring does not diffuse outward. On longer timescales, we expect the size of the gap in the dust to become progressively wider compared to that in the gas, an effect that may be detected by observations. For example, with ALMA, the spatial distribution of submillimeter emission from solids can be compared to CO observations of gas to test for possible differences in the gap sizes. If some discrepancy is detected and there is an enhanced dust emission around the outer gap edge, it may be argued that the overall gap in the disk is due to two large planets in MMR and migrating outward.

In the case of 2:1 MMR, the dust overdensity that forms at the outer border of the gap (see Figure 11) builds up at a lower rate because of the slower outward migration speed of the gas gap compared to that of the 3:2 resonance case (see Figure 1). The outer edge of the gap is also very efficient at blocking dust grains of all sizes, and only a very small fraction of the dust (of any size) crosses the outer border of the resonant gap. Almost no particle is found close to the planets, in contrast to the 3:2 MMR case, in which a non-negligible amount of dust was

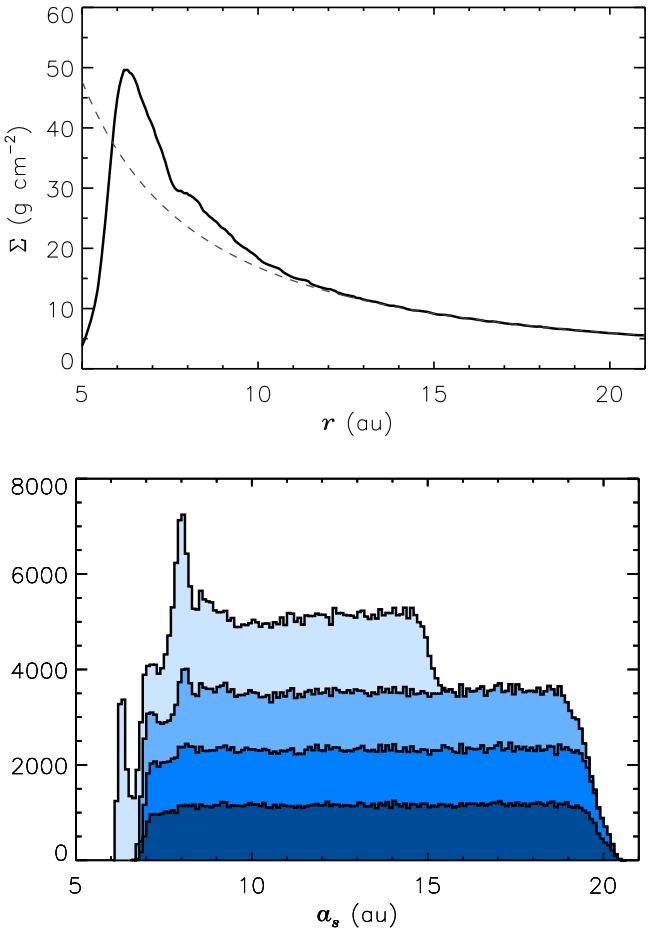

Figure 12. Top: azimuthally averaged gas surface density (solid line) exterior to a Jupiter–Saturn pair, locked in 2:1 MMR and migrating outward (see Figure 2). The dashed line represents the initial gas density distribution. Bottom: cumulative histograms of the semimajor axes of dust particles, a_s, of radii 10 μm, 100 μm, 1 mm, and 1 cm (darker to lighter colors, respectively). Note that the evolution of the grains, ≈2 kyr, is much shorter than that in Figure 11.

dragged toward the planets (compare Figure 11 with Figures 5 and 7). This suggests that at later times, the density peak at the outer edge of the gas gap will be more prominent compared to that observed in the 3:2 MMR case. This is already partly evident for the larger 1 cm size particles, which accumulate at the outer edge and build up a high-density ring during the course of the calculation (see Figure 11). The continuous supply of additional dust coming from the outer disk regions (which are not included in our model) will lead to a significant growth of the density over time. This different behavior between the two MMR configurations may provide an opportunity to distinguish between them from observations.

In Figure 12, we show results from the additional locally isothermal calculation discussed in Section 3 (see also Figure 2). The pair of planets is locked in 2:1 MMR and is migrating outward (with Jupiter and Saturn at around 2.5 and 3.97 au, respectively, at the evolution time of Figure 12). The gas surface density (top panel) is displayed starting from the outer edge of the common gas gap. The dust is initially deployed from 7 to 20 au, uniformly in radial distance and in equal numbers per size bin. The Stokes numbers at deployment range from $\approx 10^{-4}$ (for the smallest particles) to several times 10^{-2} (for the largest particles). The bottom panel shows the cumulative histogram of the semimajor axis (a_s) of particles of radii 10 μm, 100 μm, 1 mm, and 1 cm, indicated respectively by darker to lighter colors. Each colored region (i.e., the region in between two neighboring black curves) provides the actual number of particles as a function of a_s. The largest particles drift inward the fastest, as mentioned above. Inside of 6 au, the steep gas density gradient (see top panel) should efficiently push the dust outward, preventing it from reaching the interior disk. In fact, barely any particle is able to filter through the gas gap edge toward the planets.

The dust evolution shown in the bottom panel of Figure 12, ≈2 kyr, is significantly shorter than that discussed above and illustrated in Figure 11, hence the lower relative peaks at the exterior edge of the gas gap. The formation of dense dust rings is also delayed by the lower Σ of this model compared to that of the model represented in Figure 11. However, as time progresses, the density peak in the dust distribution of 1 cm grains is expected to increase. The local density of the smaller particles is also expected to increase, but on the longer timescale of the planets' outward migration (see Figure 2).

6. Discussion and Conclusions

The capture of two planets in resonance may be a common event in the early phases of evolution of planetary systems, when the circumstellar gas disk is still present. Convergent migration may drive an outer, less massive planet close to an inner more massive planet until capture occurs in either 2:1 or 3:2 MMR. The type of resonance and the subsequent evolution of the planets depend on many parameters, like the disk's surface density, the planet masses, and the disk viscosity. We focus here on a scenario where the planets, once trapped in resonance, migrate outward. This mechanism is invoked, for example, in the grand tack scenario to explain some of the properties of the inner solar system.

In this paper, we outline some peculiar traits of the dust spatial distribution produced by the perturbations of the resonant planets. These traits may produce detectable signatures, which can reveal the presence of planets in high-resolution images taken with instruments like ALMA or SPHERE (or with future instruments such as the Next Generation Very Large Array).

Through numerical models of the evolution of gas, dust, and a pair of planets with two different hydrodynamical codes, we first show that the common gas gap also induces an extended gap in the dust. This creates an ambiguity when interpreting a dust gap observed in a circumstellar disk, because the gap width can be modeled with either a single massive planet or a pair of smaller planets in resonance. However, the possible outward migration of a pair of planets locked in MMR induce some characteristic features in the dust distribution that may be used to resolve this ambiguity.

During the outward migration, the dust gap becomes progressively wider compared to the gas gap because the grains populating the region inside the inner edge of the gas gap do not move outward to refill the region behind the migrating planets. This broadening depends on the migration rate and occurs on a shorter timescale in the 3:2 MMR case compared to the 2:1 MMR case. Different disk conditions may alter this result, but capture in 2:1 MMR followed by outward migration requires a cold and low-viscosity disk. In addition, for 2:1 MMR, just after capture, the eccentricity begins to grow, leading to a progressive initial broadening of the gas gap

while it moves outward. However, even over a longer timescale, the dust gap formed by a pair of planets locked in 2:1 MMR eventually decouples from the gas gap. This behavior of the dust has two important implications. First, the inner edge of the dust gap marks the radial location at which the planets reversed the direction of their migration (assuming that inward drift of the grains due to gas drag occurs over much longer timescales). Based on estimates of gap sizes, it should be possible to deduce where the planets became locked into resonance. Second, in the case of a prolonged outward migration, the dust gap would become progressively wider, while that in the gas would approximately maintain its shape and move with the planets. Therefore, if the dust gap significantly differs from the gas gap and it is much wider, then it may be attributed to a pair of planets migrating away from the star rather than to a single (non-migrating) massive planet.

An additional feature characteristic of the outward migration of two planets locked in resonance is the formation of a high and quickly growing dust density peak at the exterior edge of the gas gap. The outward drift of the gap and the ability to trap dust act in synergy, gradually accumulating grains in a dense layer at the outer edge of the gap. This is particularly relevant for large size grains ($\sim$1 cm, Stokes numbers $\sim 10^{-2}$), whose fast inward drift contributes to collect particles at the outer edge of the gap. Also for this effect, there are significant differences between the two resonances.

In the case of the 2:1 MMR, the exterior edge of the gas gap is a very effective barrier, and dust grains are unable to cross it. Consequently, the radial drift of the gas gap pushes the dust outward and produces a significant buildup of dust, which would appear as a bright ring in high-resolution images. In the case of 3:2 MMR, the faster outward migration of the planets would lead to quicker dust accumulation at the exterior edge of the gap, but the dust barrier effect for this resonance is less effective and a significant fraction of dust particles can cross the gap and stream toward the planets, but without reaching the inner disk region. It is then expected that, for this resonance, the outer dust ring would be less prominent (in observations) compared to that produced by 2:1 resonance. If the gas density, and hence the outward migration rate, increases, then an additional peak in the dust appears, moving in from the outside and rendering the disk ring structure more complex. This additional feature is present only in the distribution of dust particles from 10 μm to 1 mm in size. In fact, almost all 1 cm grains tend to be collected around the exterior planet, once they filter through the outer edge of the gas gap.

In light of these results, what can be argued when a gap is observed in a circumstellar disk? It may be due to a single planet within a range of masses or it can be ascribed to two less massive planets locked in resonance. If they are migrating outward, then we expect two distinctive features: a decoupling between the dust and gas gap and an overdense layer at the exterior edge of the gas gap. An interesting question concerns the case of a pair of planets in MMR and migrating inward. Should we expect, in this case, too, a decoupling between the gas and dust gap with the inverted roles of the dust gap edges? The situation is not symmetric. During outward migration, dust particles at the the interior gap edge would drift inward under the action of gas drag (although on a timescale longer than the migration timescale), contributing to the broadening of the dust gap. In the case of inward migration, the dust at the exterior edge would move in the same direction as the gas gap, and the decoupling effect between the dust and gas would possibly be less conspicuous. A numerical investigation is required to get more definitive answers for some reasonable ranges of disk parameters.

The effect of gas turbulence on solids was not considered in these calculations (see, e.g., the discussion in Paardekooper & Mellema 2006; Zhu et al. 2012). Turbulence transport may induce diffusion of particles across the gap edges, possibly reducing the local density of the solids exterior to Saturn's orbit. The consequences, however, are difficult to quantify without direct simulations (and appropriate assumptions on the nature of turbulence). In fact, more generally, gas turbulence can also impact the properties of the gap edges.

An additional effect, ignored in this study, is the back-reaction of the dust particles onto the gas, which may be important when the dust-to-gas ratio grows in the proximity of the exterior border of the gap. The backreaction might alter the morphology of the gap edge, affecting the dust dynamics in this region and allowing particles to filter through. However, according to Taki et al. (2016), this may occur only when the dust-to-gas ratio approaches $\approx$1, and the restoration process of the pressure maximum is slower than the deformation process (by the dust backreaction). This may not be the case with a pressure maximum created by the competing actions of tidal forces exerted by the planets and the viscous forces exerted by the gas. This is a point, however, that deserves a dedicated investigation. It is noteworthy that the high dust density buildup at the exterior border of the gas gap may also favor accumulation and growth processes. The size distribution of the solids in this region may then be different from that of the surrounding disk, providing an additional observational test for the presence of two planets in resonance.

We thank an anonymous reviewer for helpful comments. G.D. acknowledges support from NASA's Research Opportunities in Space and Earth Science (ROSES). G.P. acknowledges support from the DFG Research Unit "Transition Disks" (FOR 2634/1, ER 685/8-1). Resources supporting the work presented herein were provided by the NASA High-End Computing (HEC) Program through the NASA Advanced Supercomputing (NAS) Division at Ames Research Center.

ORCID iDs

Francesco Marzari https://orcid.org/0000-0003-0724-9987
Gennaro D'Angelo https://orcid.org/0000-0002-2064-0801

References

Andrews, S. M., Wilner, D. J., Zhu, Z., et al. 2016, ApJL, 820, L40
Armitage, P. 2017, arXiv:1509.06382v2
Beaugé, C., Michtchenko, T. A., & Ferraz-Mello, S. 2006, MNRAS, 365, 1160
Bell, K. R., & Lin, D. N. C. 1994, ApJ, 427, 987
Birnstiel, T., Dullemond, C. P., & Brauer, F. 2010, A&A, 513, A79
Bitsch, B., Morbidelli, A., Johansen, A., et al. 2018, A&A, 612, A30
Charpinet, S., Fontaine, G., Brassard, P., et al. 2011, Natur, 480, 496
Chatterjee, S., & Ford, E. B. 2015, ApJ, 803, 33
Chatterjee, S., & Tan, J. C. 2014, ApJ, 780, 53
Crida, A., Sándor, Z., & Kley, W. 2008, A&A, 483, 325
D'Alessio, P., Calvet, N., & Hartmann, L. 2001, ApJ, 553, 321
D'Angelo, G., & Lubow, S. H. 2008, ApJ, 685, 560
D'Angelo, G., & Lubow, S. H. 2010, ApJ, 724, 730
D'Angelo, G., Lubow, S. H., & Bate, M. R. 2006, ApJ, 652, 1698
D'Angelo, G., & Marzari, F. 2012, ApJ, 757, 50
D'Angelo, G., & Podolak, M. 2015, ApJ, 806, 203

D'Angelo, G., Weidenschilling, S. J., Lissauer, J. J., & Bodenheimer, P. 2014, Icar, 241, 298
Dipierro, G., & Laibe, G. 2017, MNRAS, 469, 1932
Draine, B. T. 2011, Physics of the Interstellar and Intergalactic Medium (Princeton, NJ: Princeton Univ. Press)
Fabrycky, D. C. & Kepler Science Team 2012, AAS/Division of Dynamical Astronomy Meeting, 43, 1.03
Feldt, M., Olofsson, J., Boccaletti, A., et al. 2017, A&A, 601, A7
Ferraz-Mello, S., Beaugé, C., & Michtchenko, T. A. 2003, CeMDA, 87, 99
Hayashi, C. 1981, PThPS, 70, 35
Isella, A., Guidi, G., Testi, L., et al. 2016, PhRvL, 117, 251101
Lambrechts, M., Johansen, A., & Morbidelli, A. 2014, A&A, 572, A35
Lee, M. H. 2004, ApJ, 611, 517
Lee, M. H., & Peale, S. J. 2002, ApJ, 567, 596
Lee, M. H., & Peale, S. J. 2003, in ASP Conf. Ser. 294, Scientific Frontiers in Research on Extrasolar Planets, ed. D. Deming & S. Seager (San Francisco, CA: ASP), 197
Lissauer, J. J., Hubickyj, O., D'Angelo, G., & Bodenheimer, P. 2009, Icar, 199, 338
Marzari, F. 2018, A&A, 611, A37
Marzari, F., Baruteau, C., & Scholl, H. 2010, A&A, 514, L4
Marzari, F., & Scholl, H. 1998, A&A, 339, 278
Masset, F. 2000, A&AS, 141, 165
Masset, F., & Snellgrove, M. 2001, MNRAS, 320, L55
Mihalas, D., & Weibel Mihalas, B. 1999, Foundations of Radiation Hydrodynamics (New York: Dover)
Mills, S. M., Fabrycky, D. C., Migaszewski, C., et al. 2016, Natur, 533, 509
Moorhead, A. V., & Adams, F. C. 2005, Icar, 178, 517
Morbidelli, A., & Crida, A. 2007, Icar, 191, 158
Movshovitz, N., Bodenheimer, P., Podolak, M., & Lissauer, J. J. 2010, Icar, 209, 616
Müller, T. W. A., & Kley, W. 2012, A&A, 539, A18
Mustill, A. J., & Wyatt, M. C. 2011, MNRAS, 413, 554
Paardekooper, S.-J., & Mellema, G. 2004, A&A, 425, L9
Paardekooper, S.-J., & Mellema, G. 2006, A&A, 453, 1129
Petigura, E. A., Sinukoff, E., Lopez, E. D., et al. 2017, AJ, 153, 142
Picogna, G., & Kley, W. 2015, A&A, 584, A110
Picogna, G., Stoll, M. H. R., & Kley, W. 2018, A&A, 616, A116
Pierens, A., & Nelson, R. P. 2008, A&A, 482, 333
Pierens, A., Raymond, S. N., Nesvorny, D., & Morbidelli, A. 2014, ApJL, 795, L11
Pinilla, P., Birnstiel, T., Ricci, L., et al. 2012, A&A, 538, A114
Pringle, J. E. 1981, ARA&A, 19, 137
Quillen, A. C. 2006, MNRAS, 365, 1367
Ragusa, E., Rosotti, G., Teyssandier, J., et al. 2018, MNRAS, 474, 4460
Rein, H., Papaloizou, J. C. B., & Kley, W. 2010, A&A, 510, A4
Ricci, L., Liu, S.-F., Isella, A., & Li, H. 2018, ApJ, 853, 110
Rice, W. K. M., Armitage, P. J., Wood, K., & Lodato, G. 2006, MNRAS, 373, 1619
Rosotti, G. P., Juhasz, A., Booth, R. A., & Clarke, C. J. 2016, MNRAS, 459, 2790
Steffen, J. H., Fabrycky, D. C., Agol, E., et al. 2013, MNRAS, 428, 1077
Stone, J. M., & Norman, M. L. 1992, ApJS, 80, 753
Taki, T., Fujimoto, M., & Ida, S. 2016, A&A, 591, A86
Tanaka, H., Takeuchi, T., & Ward, W. R. 2002, ApJ, 565, 1257
Teyssandier, J., & Terquem, C. 2014, MNRAS, 443, 568
Thommes, E. W. 2005, ApJ, 626, 1033
Walsh, K. J., Morbidelli, A., Raymond, S. N., O'Brien, D. P., & Mandell, A. M. 2011, Natur, 475, 206
Weidenschilling, S. J. 1977, MNRAS, 180, 57
Wright, J. T., Veras, D., Ford, E. B., et al. 2011, ApJ, 730, 93
Zhu, Z., Nelson, R. P., Dong, R., Espaillat, C., & Hartmann, L. 2012, ApJ, 755, 6
Zhu, Z., Stone, J. M., Rafikov, R. R., & Bai, X.-n. 2014, ApJ, 785, 122